

Size-Dependent Cell Uptake of Protein-Coated Graphene Oxide Nanosheets

Qingxin Mu,[†] Gaoxing Su,^{†,‡} Liwen Li,^{†,‡} Ben O. Gilbertson,[§] Lam H. Yu,[§] Qiu Zhang,[‡] Ya-Ping Sun,[⊥] and Bing Yan^{*,†,‡}

[†]Department of Chemical Biology & Therapeutics, St. Jude Children's Research Hospital, Memphis, Tennessee, 38105, United States

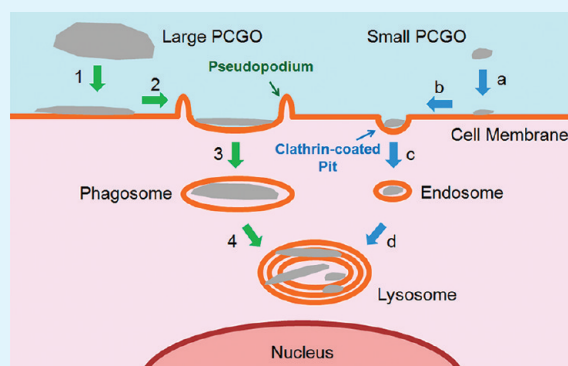
[‡]School of Chemistry and Chemical Engineering, Shandong University, Jinan, China, 250100

[§]Department of Physics, University of Memphis, Memphis, Tennessee, 38152, United States

[⊥]Department of Chemistry and Laboratory for Emerging Materials and Technology Hunter Hall, Clemson University, Clemson, South Carolina, 29634-0973, United States

S Supporting Information

ABSTRACT: As an emerging applied material, graphene has shown tremendous application potential in many fields, including biomedicine. However, the biological behavior of these nanosheets, especially their interactions with cells, is not well understood. Here, we report our findings about the cell surface adhesion, subcellular locations, and size-dependent uptake mechanisms of protein-coated graphene oxide nanosheets (PCGO). Small nanosheets enter cells mainly through clathrin-mediated endocytosis, and the increase of graphene size enhances phagocytotic uptake of the nanosheets. These findings will facilitate biomedical and toxicologic studies of graphenes and provide fundamental understanding of interactions at the interface of two-dimensional nanostructures and biological systems.



KEYWORDS: graphene oxide nanosheets, protein binding, cell uptake, clathrin-mediated endocytosis, phagocytosis, size dependence

INTRODUCTION

Graphene, a hexagonal carbon nanostructure similar to carbon nanotubes and fullerene, has unique electronic, thermal, and mechanical properties, showing tremendous application potential in fields such as electronics and biomedicine.^{1,2} Graphene oxide (GO), which is oxidized graphite with enhanced aqueous solubility, has been proven to be an efficient biosensor,³ drug carrier,^{4,5} and photothermal cancer-killing agent.^{6,7} GO nanosheets are able to enter cells which renders them to become promising candidates for intracellular delivery of drugs and cellular imaging. However, the mechanisms of how the emerging nanostructures interface with biological systems are still largely unknown. In particular, a fundamental understanding of its ability to penetrate cell membranes and other biological barriers is still lacking. For instance, whether the nanosheets parallelly attach onto cell surface or vertically insert into cell membrane? By what manner they enter cells? Such cellular uptake properties of nanoparticles may affect cell signaling, proliferation, differentiation, and nanoparticle excretion.^{8–10} Cellular uptake of nanoparticles with other shapes has been studied.¹¹ We and other researchers previously discovered endosomal leakage and nuclear translocation of multiwalled carbon nanotubes.^{9,12} However, the behavior of sheet-shaped nanostructures has not been reported. Furthermore, the effect of size on cellular uptake of this type of applied

materials is also poorly understood. Such a knowledge gap may impede further biomedical development of graphene and its derivatives.

In this study, we aimed to elucidate the cellular uptake mechanisms of the novel material. We report a detailed investigation of the cell uptake of protein-coated GO nanosheets (PCGO). Using various labeling techniques and microscopic methods, we observed cell-surface adhesion of PCGO, plasma membrane invagination, and intracellular vesicle formation in a model cell line. We further separated PCGO by size and discovered that protein-coated large and small size GO nanosheets are taken up by cells predominantly through phagocytosis and clathrin-mediated endocytosis (CME), respectively. These findings provide fundamental understanding of how graphene nanosheets interface with cell membrane and size-dependent cellular uptake mechanisms, which will facilitate both their nanomedicine and nanotoxicity studies.

EXPERIMENTAL SECTION


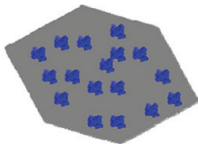
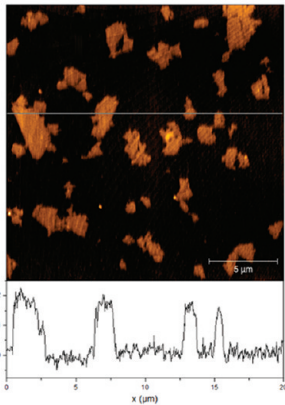
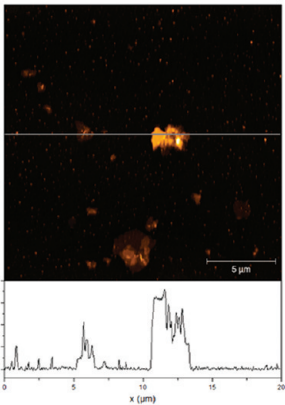
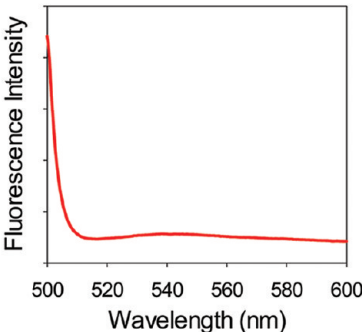
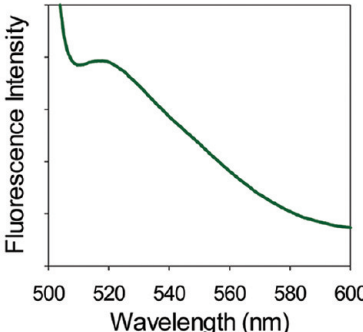
Materials. GO nanosheets were purchased from Cheaptubes.com (Brattleboro, VT). Mouse mesenchymal progenitor C2C12 cells (from

Received: February 13, 2012

Accepted: March 13, 2012

Published: March 13, 2012

Table 1. Characterization of GO and PCGO Nanosheets

	GO	PCGO
Schematic ^a		
Atomic Force Microscopy		
Fluorescence Spectrum		
ζ-Potential ^b	−48.8 mV (W); −10.4 mV (M)	−40.3 mV (W); −9.98 mV (M)
Protein density ^c	0/μm ²	~10000/μm ²

^aGray sheets indicate GO and blue spots indicate FITC-BSA. ^bW and M represent water and cell culture medium, respectively. ^cThe density is shown as the estimated number of proteins per square micrometer on nanosheets. The calculation is based on the quantity of proteins and the surface area of GO.¹³

ATCC, Manassas, VA) were grown in Dulbecco's Minimum Essential Medium (DMEM, Gibco, Grand Island, NY) supplemented with 10% heat-inactivated fetal bovine serum (Invitrogen, Carlsbad, CA), 10% FBS, 2 mM L-glutamine, 100 U/mL penicillin, and 100 μg/mL streptomycin. Chemicals were purchased from Acros Organics (Geel, Belgium), Sigma-Aldrich (St. Louis, MO), or otherwise indicated and were used without further purification.

Labeling of GO by Fluorescein Isothiocyanate-Modified Bovine Serum Albumin (FITC-BSA) and Characterizations.

1. Labeling. GO and FITC-BSA were dissolved in H₂O (Milli-Q, 18.2 MΩ) with concentrations of 2 mg/mL, respectively. GO and FITC-BSA solutions were mixed with mass ratio of 1:1 with gentle pipetting. The mixture was then incubated at 37 °C overnight and centrifuged at 16 000g for 30 min at 4 °C. The pellet was then washed 3 times with PBS and centrifuged at 16 000g, 10 min each time. The resulting pellet was resuspended in H₂O and stored in a refrigerator. The PCGO complex was used in the same day of preparation for all assays.

2. Steady State Fluorescence Spectroscopy. Steady state fluorescence spectra of GO and PCGO were measured using a

Hitachi F-7000 spectrofluorometer (Hitachi Co. Ltd., Tokyo, Japan). Samples were excited at 488 nm and emission wavelength was set from 500 to 600 nm. Scanning speed was 1200 nm/min. Excitation and emission slit was set to 5.0 and 10.0 nm, respectively. PMT voltage was set to 950 V. Measurements were performed at room temperature (23 °C).

3. Atomic Force Microscopy (AFM). Size and thickness of GO and PCGO were measured by AFM. Aqueous solutions of GO for each experimental condition were prepared at a concentration of 0.25 mg/mL and spin-coated on silicon dioxide surfaces measuring about 12 mm square. The SiO₂ was cleaned in argon plasma for at least 10 min prior to spin coating. Spin coating was performed for 5.5 min at 3500 rpm with 75 μL of sample solution (enough to completely wet the cleaned SiO₂ surface). Imaging was performed using a Nanosurf easyScan 2 AFM operated in tapping mode with VISTAProbes T190R 190kHz cantilevers. Image analysis was performed using the SPM analysis software Gwyddion (<http://gwyddion.net>).

4. Zeta-Potential Measurement. The zeta-potential of GO and PCGO was determined using Zetasizer Nano-Z (Malvern Instruments, Worcestershire, UK). The analysis was performed at 25.0 ± 0.2 °C

using sample solutions in Milli-Q water or cell culture medium. The zeta-potential was an average of three independent measurements.

Scanning Electron Microscopic (SEM) Characterization of Cell Surface Adhesion by PCGO. Cells were seeded onto Thermanox coverslips (NUNC, Rochester, NY) which were put on bottoms of a 6-well plate. PCGO stock solution was added into cell culture medium to a final concentration of 20 $\mu\text{g}/\text{mL}$. Control cells were only fed with medium. After 30 min, cells were washed with PBS and then fixed with 2.5% (v/v) glutaraldehyde (buffered in 0.1 M sodium cacodylate) overnight. The cells were then postfixed with 1% osmium tetroxide for 1 h. The samples were then dehydrated through a series of alcohol concentrations (35%, 50%, 70%, 90%, and 95%) followed by further dehydration with 100% ethanol and then dried in carbon oxide in a desiccator. The samples were then mounted onto SEM aluminum stubs and sputter coated with Au/Pd and then analyzed using the Philips XL 30 ESEM (FEI Company, Portland, OR).

Confocal Laser Scanning Microscopic (CLSM) Characterization of Cellular Uptake of PCGO. C2C12 cells were incubated with PCGO (20 $\mu\text{g}/\text{mL}$) for 30 min. Cells were then fixed with 4% paraformaldehyde (PFA) for 1 h at room temperature and stained with 10 $\mu\text{g}/\text{mL}$ WGA-Alexa Fluor 647 (Invitrogen, Carlsbad, CA) for 5 min followed by 3 times of PBS washing (5 min each). Cells were then mounted with VECTASHIELD mounting medium (with DAPI) (Vector Laboratories, Inc. Burlingame, CA) at 4 $^{\circ}\text{C}$ overnight. The images were analyzed using Laser Scanning Microscope LSM 510, Version 3.2 SP2 (Carl Zeiss GmbH, Germany).

Flow Cytometric Measurement of Cellular Uptake. Cells incubated with PCGO were washed with cold PBS for 3 times followed by Trypsin digestion. Cells were suspended in culture medium for flow cytometric analyses. Flow cytometry analyses were performed on a Guava EasyCyte Mini flow cytometry system (Millipore, Billerica, MA).

Separation and Characterization of Large and Small PCGO. PCGO solution in H_2O was centrifuged at 2000g for 5 min. The pellet (PCGO1) was collected and resuspended in H_2O . The supernatant was centrifuged at 10 000g for 5 min, and the resulting pellet was discarded. The resulting supernatant was collected and filtrated through a 5 kDa ultrafiltrate concentrator (Corning, Inc., Corning, NY). The concentrate was named as PCGO2. The concentration of PCGO was measured by absorbance at 600 nm. (Absorption of FITC-BSA was undetectable at this wavelength, and the absorption of PCGO obeys Beer–Lambert law.)

Synthesis and Characterization of 5 nm Gold Nanoparticles (GNPs) and Labeling of PCGO. Milli-Q water (90 mL) and $\text{HAuCl}_4 \cdot 3\text{H}_2\text{O}$ stock solution (1 mL, 10 mg/mL) were added in a 200 mL flask with a vigorous stirring. Next, sodium citrate solution (2 mL, 38.8 mM) was added and stirred for 1 min. NaBH_4 (0.75 mg) in 38.8 mM sodium citrate solution (1 mL) was then added and stirred for 5 min. The obtained GNPs solution was concentrated to 0.5 mg/mL with an ultrafiltration tube (MWCO: 5000) as stock solution. GNPs were characterized by TEM and UV–vis absorption spectroscopy.

Labeling of PCGO was completed by mixing PCGO and GNP solutions with mass ratio of 1:1 followed by gentle shaking for 20 min. The complex was stored in a refrigerator and used in the same day of preparation. Attachment of GNPs onto PCGO was confirmed by TEM observation.

Transmission Electron Microscopic (TEM) Characterization of Cellular Uptake of Large and Small PCGO. C2C12 cells were treated with 50 $\mu\text{g}/\text{mL}$ (amount of PCGO) GNP-labeled PCGO for 30 min. Then, cells were fixed in 2.5% glutaraldehyde in 0.1 M sodium cacodylate buffer (pH 7.4) for 1 h in room temperature and rinsed. Cells were then post fixed 1 h in 2% osmium tetroxide with 3% potassium ferrocyanide and rinsed, next enbloc staining with a 2% aqueous uranyl acetate solution and dehydration through a graded series of alcohol, two changes of propylene oxide, a series of propylene oxide/Epon dilutions, and embedded in 100% Epon. The thin (70 nm) sections were cut on a Leica UC6 ultramicrotome, and images were taken on a JEOL 1200 EX (JEOL, Ltd. Tokyo, Japan) using an AMT 2k digital Camera.

Quantification of Cellular Uptake of Large and Small PCGO with Different Inhibitors. Cells were treated with 0.1% $\text{NaN}_3/50$ mM 2-deoxyglucose or cytochalasin D (5 $\mu\text{g}/\text{mL}$) in serum-free DMEM (0.1% BSA) for 1 h before incubation of PCGO (50 $\mu\text{g}/\text{mL}$) with inhibitor in the fresh media for 1 h. For chlorpromazine, cells were preincubated in serum-free DMEM (0.1% BSA) containing 10 $\mu\text{g}/\text{mL}$ chlorpromazine for 30 min at 37 $^{\circ}\text{C}$. The media was then changed to fresh media containing the inhibitors plus PCGO (20 $\mu\text{g}/\text{mL}$) and further incubated for 1 h. Cells were then washed, trypsinized, and analyzed by flow cytometry.

RESULTS AND DISCUSSION

Labeling of GO with Protein. Single- or multi-layered GOs are intrinsically undetectable by various microscopic techniques in biological environments such as a cell. Moreover, the dispersibility of GO in physiological solutions is rather low because of the high ionic strength of such solutions. To overcome such difficulties, we took advantage of the strong protein-binding capability of GO and labeled the nanosheets with FITC-BSA. Because of the size of BSA molecule, the direct interactions between FITC and GO and, therefore, the quenching of fluorescence can be minimized. We have used the material for labeling of carbon nanotubes and made them green fluorescent in live cells.^{9,10} Similarly, the labeled PCGO was also fluorescent (Table 1) and highly dispersible in cell culture medium. The binding barely changed the surface potential of GO in water (−48.8 to −40.3 mV). In cell culture medium, the ζ -potentials of GO and PCGO nanosheets are similar (approximately −10 mV), indicating that more protein binding occurred for both nanosheets. AFM images showed that, compared to GO (1.8 \pm 0.9 nm), PCGO nanosheets had a maximum thickness of 9.1 \pm 7.1 nm (Table 2), indicating that

Table 2. Statistical Size Distribution Analysis of GO and PCGO Based on Atomic Force Microscopy Measurements

sample name	equivalent disk diameter (mean \pm SD) (μm) ^a	minimum height per nanosheet (mean \pm SD) (nm)	maximum height per nanosheet (mean \pm SD) (nm)	average height on nanosheet surface (nm) ^b
GO	0.84 \pm 0.41	0.5 \pm 0.3	1.8 \pm 0.9	1.1
PCGO	0.63 \pm 0.35	1.1 \pm 0.2	9.1 \pm 7.1	3.9
PCGO1	0.86 \pm 0.37	1.2 \pm 0.6	9.6 \pm 7.2	5.2
PCGO2	0.42 \pm 0.26	1.1 \pm 0.3	5.2 \pm 3.2	3.2

^aThe equivalent disk diameter data were skewed, and the Box-Cox transformation was applied to yield a more normal distribution.²⁴ The standard deviations of the transformed data were retransformed back to the original data scale to obtain the reported standard deviation values. ^bAverage height was measured across the surface area of all nanosheets.

proteins were binding to GO and increasing its thickness. When equal masses of GO and FITC-BSA were mixed, no protein was detected in the supernatant after centrifugation, indicating that all proteins were adsorbed onto GO (Figure S1 in Supporting Information). Therefore, the mass ratio of GO to FITC-BSA is approximately 1:1. Using the molecular weight of the protein (~67 kDa) and the surface area of graphene (~900 m^2/g),¹³ we calculated that there were approximately 10 000 protein molecules in one square micrometer of nanosheets. Since PCGO was used in all assays cellular study, we tested the stability of the complex. Results showed that PCGO can be well-dispersed in cell culture medium (Figure 11), and no

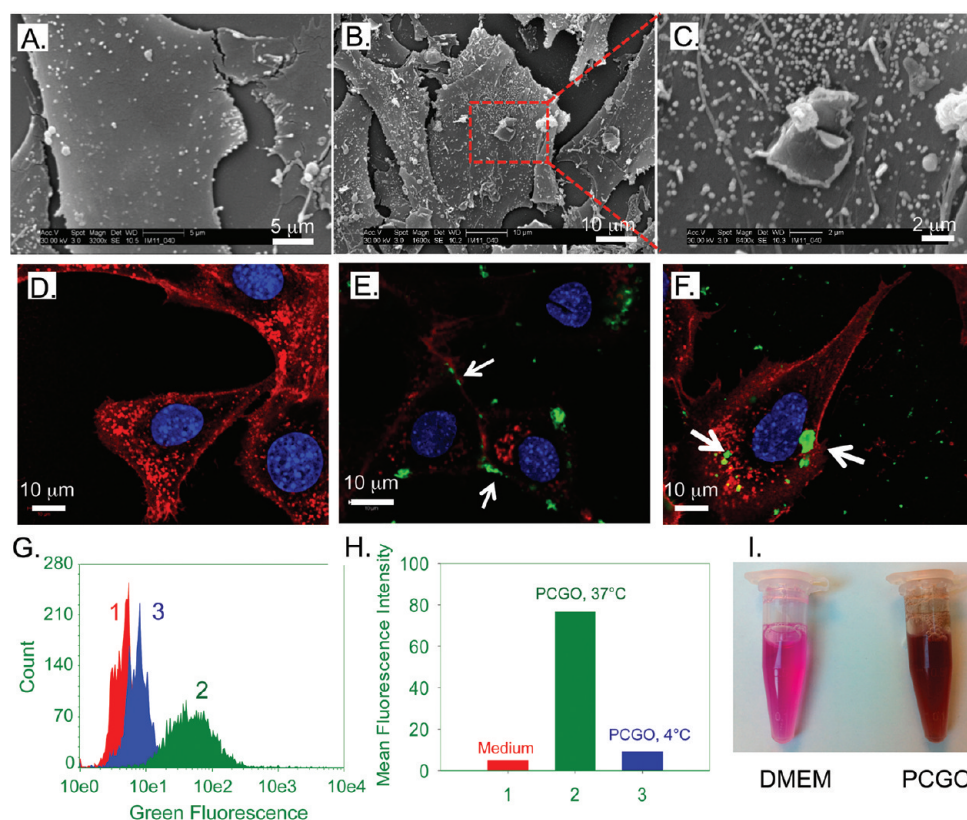


Figure 1. Cell surface adhesion and energy-dependent uptake of PCGO nanosheets. (A–C) Scanning electron microscopy micrographs of C2C12 cells with medium only (A) and after 30 min incubation with PCGO (20 $\mu\text{g}/\text{mL}$). (B) A closer view indicating adhesion of one piece of PCGO on the cell surface (C). (D–F) Confocal microscopic images of C2C12 cells with medium only (D) and after 30 min incubation with PCGO (20 $\mu\text{g}/\text{mL}$) (E) PCGO on cell surface and (F) PCGO in cells. Arrows indicate PCGO. Red: cell membrane; blue: nucleus; green: PCGO. (G) Flow cytometry measurements of C2C12 cells with medium only (1), 20 $\mu\text{g}/\text{mL}$ PCGO for 30 min at 37 $^{\circ}\text{C}$ (2) or PCGO (20 $\mu\text{g}/\text{mL}$) for 30 min at 4 $^{\circ}\text{C}$ (3), as indicated. (H) Mean fluorescence intensities of conditions (1), (2), and (3). (I) Photographs of DMEM complete cell culture medium (left) and PCGO suspension in the medium (right).

FITC-BSA was released from GO for at least 24 h (Figure S2 in Supporting Information).

Cell Surface Adhesion of PCGO. Cellular uptake mechanisms of nanoparticles having various shapes have been reported. For instance, spherical nanoparticles enter cells through CME, caveolae-mediated endocytosis, phagocytosis, or macropinocytosis, which all require energy.^{14–16} Tubular nanoparticles enter cells through endocytosis or energy-independent direct penetration.^{17,18} All these processes require that nanoparticles attach to the cellular membrane before engulfment or insertion.¹⁹ Unlike spherical or tubular nanoparticles, GO has large flat surfaces with irregular shapes. Additionally, the flexibility and folding properties of GO's thin layers make them act as gauzelike shapes in biological medium. GO has been reported to be an efficient intracellular transporter for drug and gene delivery, indicating that it can efficiently enter cells.² On the basis of these observations, we hypothesized that GO adheres to the cell surface and is then internalized.

Driven by our preliminary hypothesis, we first investigated whether PCGO could attach to the surface of cells and in what orientation this occurred. A model cell line C2C12 (mouse mesenchymal progenitor) was selected in this study. Upon SEM examinations, large PCGO pieces were frequently observed adhering face to face onto the cell surface (Figure 1B,C). We never observed any PCGO and cells binding perpendicularly. On the basis of SEM observations, previous

report on nanoparticle–cell interactions, and properties of PCGO, we speculate that the adhesion is a result of several factors. First, the similar curvature between the nanosheets and plasma membrane would facilitate their holding together. Second, there are multiple binding forces between them, including electrostatic and hydrophobic interactions between nanosheets and phospholipid bilayers. Third, there could be specific ligand–receptor interactions between proteins bound to PCGO and membrane receptors. This factor might induce receptor-mediated endocytosis of PCGO. On the basis of $\sim 10\,000$ BSA molecules per square micrometer area of GO (AFM studies) and the cross section of BSA $\sim 14 \times 4 \times 4$ nm, we estimate that the average BSA coverage on the graphene oxide surface to be 43%. Therefore, although the density of protein molecules on GO surface is high, there is still space on GO surface to facilitate the direct interactions of GO with cell membrane structures. A detailed understanding on the driving forces for the cell uptake requires future studies. Limited by resolution of SEM on cells, small PCGO pieces could not be identified. However, the attachment propensity of PCGO revealed a unique interaction mode between two-dimensional nanostructures with cells.

Cell Uptake of PCGO without Cytotoxicity. SEM observations provided clear pictures of how PCGO nanosheets were attached to the cell surface. To further investigate how PCGO nanosheets altered cell membranes and entered cells, we used other techniques. Because PCGO was fluorescent, we

used confocal microscopy to investigate the cell attachment and engulfment of nanosheets. Fluorescent particles were found on the cell membranes (labeled by thin arrows), consistent with SEM observations (Figure 1E). The green fluorescent particles inside cells (labeled by thick arrows) indicate that the nanosheets enter cells after surface adhesion (Figure 1F). The results also indicate that PCGO can enter cells as fast as 30 min. After reviewing the likely cell uptake mechanisms of nanoparticles with various shapes, we speculate that the cellular entrance of PCGO is an energy-dependent process. Such process is temperature dependent. Next, we measured the cellular uptake of PCGO at 37 and 4 °C using flow cytometry. Mean fluorescence intensity (MFI) signified the relative amount of PCGO taken up by cells. The result showed that more than 80% of PCGO internalization was inhibited at 4 °C (Figure 1G,H), indicating that this is an energy-dependent process. Because the adhesion of PCGO on cell surface cannot be inhibited at low temperature, this study also showed that the fluorescence measurement by flow cytometry best describes internalized PCGOs in cells. To understand whether the uptake of PCGO caused toxicity in C2C12 cells, we examined cytotoxicity using the WST-1 assay which measures metabolic activity of live cells. Results showed that PCGO caused very little inhibition of cell proliferation at doses up to 100 $\mu\text{g}/\text{mL}$ (Figure S3 in Supporting Information). Despite that some reports showed toxicity of GO to mammalian cells, the coating of proteins on GO might mitigate its cytotoxicity in mammalian cells. The preincubation of GO (100 $\mu\text{g}/\text{mL}$) with fetal bovine serum improved cell viability in A549 cells by as much as 20% as compared to GO.²⁰

Size-Dependent Cell Uptake of PCGOs. Size dependence of cellular uptake is a crucial issue that needs to be examined for various nanoparticles.^{21–23} It is still not known whether uptake of PCGO is size dependent. To explore the dependence of cell intake amount and internalization pathways on particle size, we fractionated PCGO by centrifugations. Large (PCGO1) and small (PCGO2) protein-coated nanosheets were separated and characterized using TEM and AFM, respectively (Figure 2A,B). Since PCGO nanosheets were stable as aforementioned, we do not expect any protein loss during the separation process. Size distributions of large and small nanosheets were obtained by AFM measurements and analyzed statistically.²⁴ Since the shape of nanosheets was irregular, to facilitate the quantifications, we assumed that all PCGO nanosheets were round-shaped. The area of nanosheets was analyzed on the basis of AFM results. The equivalent disk diameter calculated from the area was used to indicate the size of nanosheets. On average, PCGO1 was 2-fold larger than PCGO2 on the basis of assumed equivalent disk diameter (Table 2). On the basis of density of proteins on nanosheets and nanosheets' sizes, one can estimate that the average numbers of proteins on PCGO1 and PCGO2 were approximately 11 600 and 2800, respectively.

We quantitatively measured the cellular uptake of PCGO1 and PCGO2 at 1, 2, and 14 h using flow cytometry. The cellular uptake of PCGO was both time and size dependent (Figure 2C). In a relatively short period of incubation (1 h), the fluorescence signal from PCGO1 nanosheets was stronger than that from PCGO2, probably due to the larger surface area of PCGO1 and its having more bound fluorescent proteins per sheet. However, PCGO2's fluorescence surpassed that of PCGO1 with time, indicating much more accumulation of small PCGO in cells. One possibility is that large and small

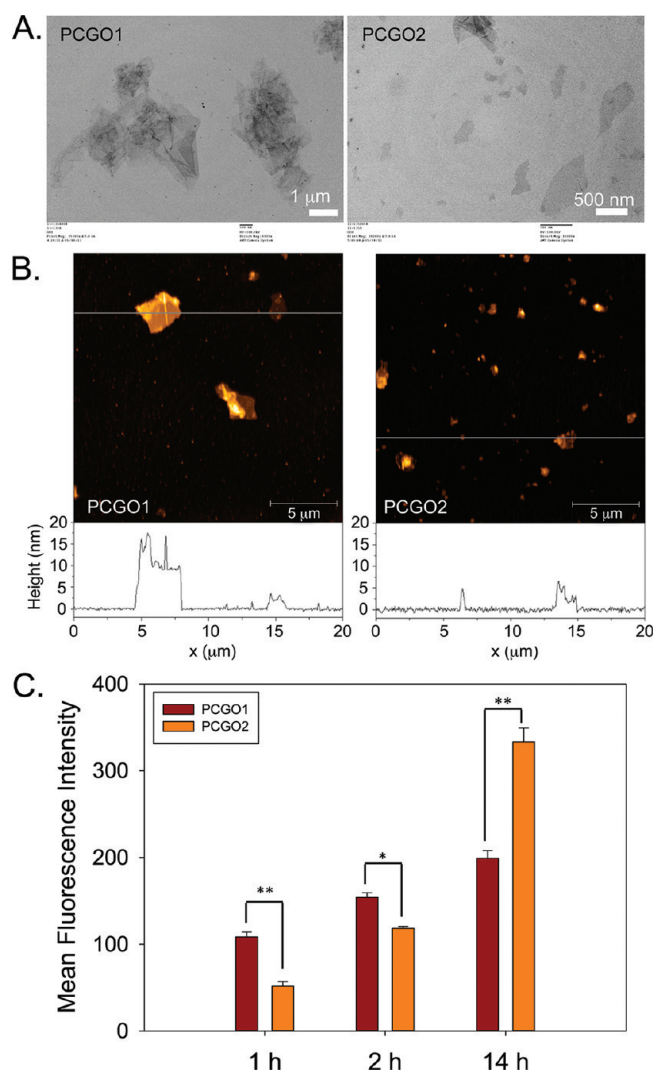


Figure 2. Characterization of large and small PCGO nanosheets and their size-dependent cellular uptake. (A) Transmission electron microscopic photographs. Scale bars represent 1 μm for PCGO1 and 500 nm for PCGO2. (B) Atomic force microscopic images. Scale bars represent 5 μm . (C) Quantification of uptake by flow cytometry. C2C12 cells incubated with PCGO1 or PCGO2 (50 $\mu\text{g}/\text{mL}$) for 1, 2, or 14 h, as indicated. *, $p < 0.05$; **, $p < 0.01$.

nanosheets entered cells at similar rates, with smaller nanosheets being less fluorescent because they bound fewer FITC-BSA molecules. Over time, many more small nanosheets than large nanosheets were engulfed.

Next, we examined the subcellular locations of PCGO using TEM (Figure 3). Since PCGO has a low electron density, it is difficult to distinguish nanosheets from other cellular components using TEM (data not shown). To resolve this issue, we used PCGO labeled with GNPs (5 nm) to guide the observation (Figure S4 in Supporting Information). GNPs can bind onto proteins on GO nanosheets through electrostatic interactions²⁵ and were not released within at least 2 h (Figure S5 in Supporting Information). Size-dependent cellular uptake of PCGO–GNP after 1 h of incubation was quantitatively determined using inductively coupled plasma mass spectrometry (ICP-MS) according to the procedure we previous used for GNPs array study.^{26–28} The cellular uptake amounts were similar whether determined using ICP-MS or flow cytometry (Figure S6 in Supporting Information) for both PCGO1 and PCGO2.

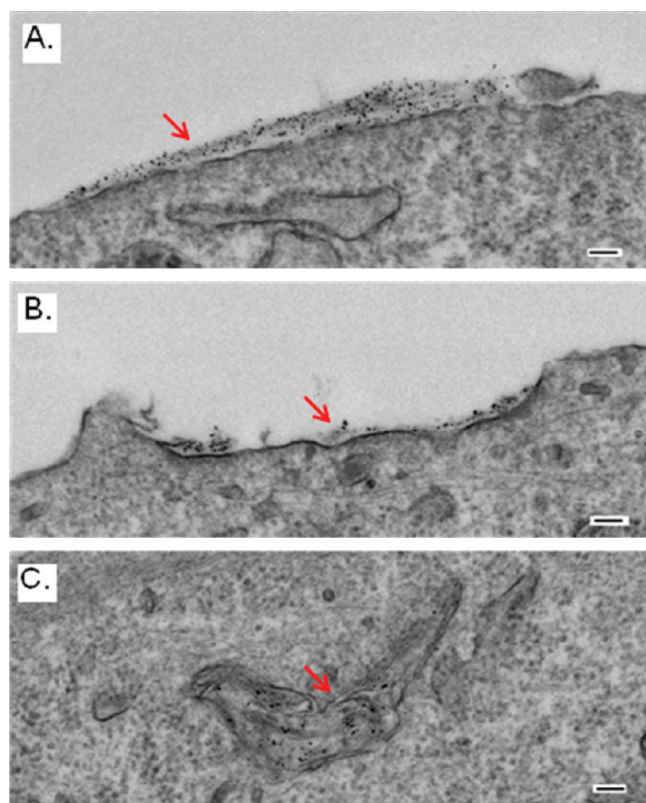


Figure 3. Ultrastructural examination of C2C12 cells incubated with GNP-labeled PCGO1 ($50 \mu\text{g/mL}$, 30 min). (A) PCGO1 adhered on the cell surface, (B) in cell invaginations, and (C) in intracellular vesicles. Red arrows indicate GNP-labeled PCGO1. The scale bars represent 100 nm.

These data indicate that the cellular uptake of different sized PCGO have the same pattern with GNP-labeled PCGO. Therefore, uptake of PCGO was not affected by GNP labeling. Stages of internalization of large and small nanosheets were observed on TEM images. After nanosheets attached to cell membranes (Figures 3A and 4A), membranes underwent specialization, invagination (Figures 3B and 4B), and vesicle formation (Figures 3C and 4C). The observed membrane attachment of large PCGO was consistent with observations made using SEM and CLSM. The membrane invaginations observed in Figures 3B and 4B indicate the features of phagocytosis and CME, respectively. The existence of PCGO in cellular vesicles was also consistent with our CLSM observations. PCGO was not found in cytoplasm, mitochondria, or nucleus in this study. However, the wrapping of large PCGO nanosheets onto a pseudopodium was observed (Figure S7 in Supporting Information), indicating that cellular migration and feeding processes might be disrupted.

Endocytosis of Large PCGOs Is Steered toward More Phagocytosis. On the basis of the outlined observations, we hypothesized that PCGOs of different sizes have different uptake mechanisms. To examine this, we quantified the cell uptake of both large and small PCGO nanosheets after incubating the cells with inhibitors of energy-dependent cell uptake, phagocytosis, and CME (Figure 5). A mixture of sodium azide and 2-deoxyglucose (NaN_3/DOG) depleted ATP in cells and inhibited approximately 80% of cellular uptake of PCGOs, regardless of their size. This result suggests that almost all nanosheets had entered the cells using energy-dependent

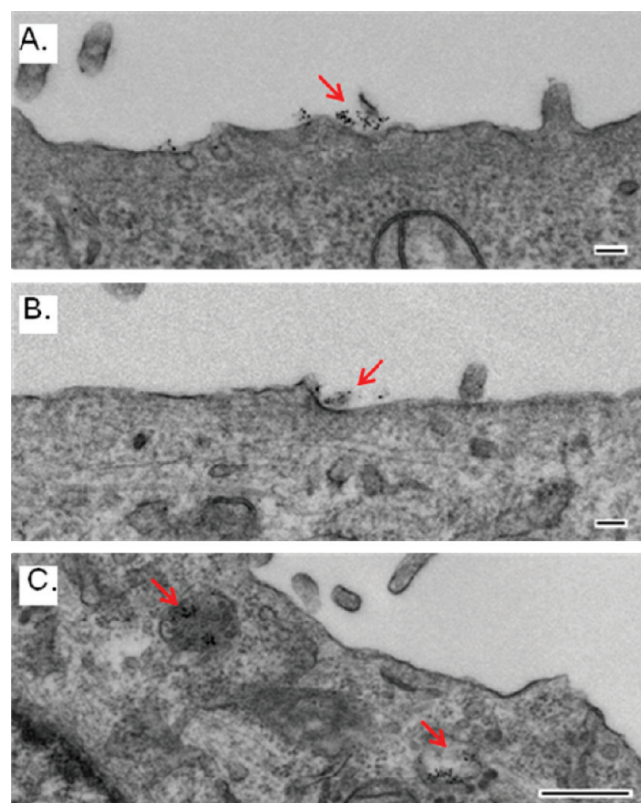


Figure 4. Ultrastructural examination of C2C12 cells incubated with GNP-labeled PCGO2 ($50 \mu\text{g/mL}$, 30 min). (A) PCGO2 adhered on the cell surface, (B) in cell invaginations, and (C) in intracellular vesicles. Red arrows indicate GNP-labeled PCGO2. The scale bars represent 100 nm in A and B and 500 nm in C.

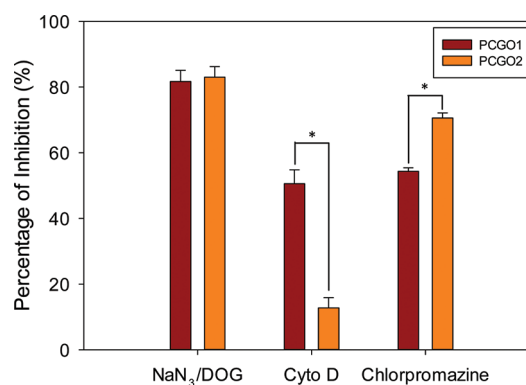


Figure 5. Inhibition of cellular uptake by various inhibitors. The percentage of inhibition was generated from the ratios between mean fluorescence intensities of cells incubated with PCGOs ($50 \mu\text{g/mL}$) for 1 h with and without various inhibitors. All results are expressed as mean \pm SD; *, $p < 0.05$.

processes, consistent with the uptake of pooled PCGO at 4°C (Figure 1G,H). Cytochalasin D (Cyto D) inhibits actin polymerization and actin microfilaments formation. It inhibits phagocytosis in cells that possess partial or full phagocytotic function.²⁹ C2C12 cells are known to possess phagocytotic activity.³⁰ Cyto D inhibited cell uptake in a size-dependent manner (Figure 5). It inhibited the uptake of PCGO1 much stronger than it did that of PCGO2, indicating that larger nanosheets entered cells predominantly through phagocytosis. Chlorpromazine, a Rho GTPase and CME inhibitor,³¹ reduced

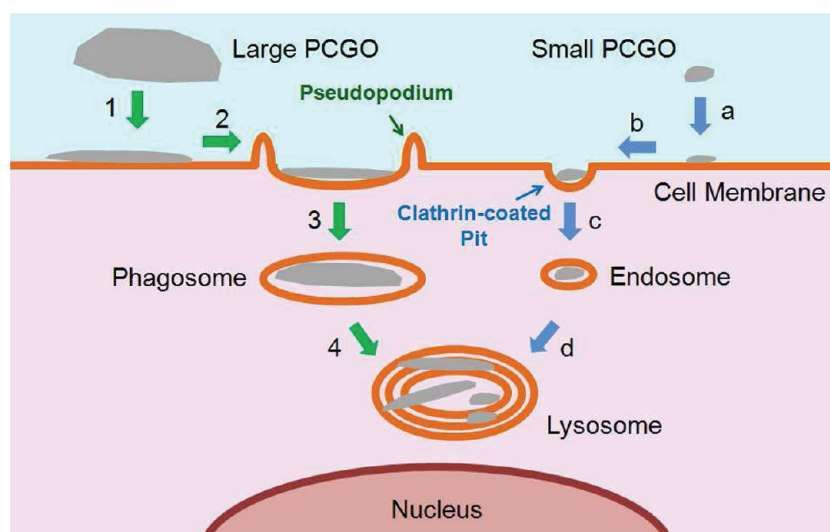


Figure 6. A working model for cell uptake of PCGO. Numbers (1–4) and letters (a–d) indicate different steps of large and small nanosheets internalizing into cells, respectively.

the uptake of all PCGO nanosheets, yet the inhibition of PCGO2 was much stronger than that of PCGO1, indicating that smaller PCGO nanosheets entered cells primarily through CME. Our TEM observations, flow cytometric quantification, and inhibition assay results collectively showed that protein-coated small nanosheets enter cells through CME, while large nanosheets use both CME and phagocytosis. Because there is still no detailed description of cellular uptake mechanisms of two-dimensional nanosheets, we propose a working model for the cellular uptake of large and small PCGOs (Figure 6). For large PCGO, the nanosheets first attach onto cell surface followed by membrane invagination and extending of pseudopodia and are subsequently engulfed into phagosome. For small PCGO, the nanosheets attach onto cell surface followed by formation of clathrin-coated pits and are subsequently engulfed into endosome. All nanosheets enter lysosomes for excretion. The cellular uptake properties of different sizes of PCGO provide insight into the bioactivity of these nanostructures that can be used in designing biomedical devices. Large nanosheets may preferentially translocate into the reticuloendothelial system, and small nanosheets are capable of being distributed in various organs. The *in vitro* and *in vivo* activity of GO nanosheets may be regulatable by controlling their size. Such hypothesis is consistent with recent studies.^{32,33} In an *in vitro* study, small GO induced much more cell viability loss than large ones.³² In an *in vivo* study, it was reported that smaller sized surface functionalized graphene nanosheets have lower liver and spleen distribution compared to larger ones, which enhances their relative tumor accumulation and makes them a promising photothermal therapy agent.³³

CONCLUSIONS

In summary, our results reveal that sheet-shaped GO nanostructures with protein coating are able to adhere onto cell surfaces and undergo size-dependent internalization. Protein-coated small nanosheets enter cells mainly through CME while protein-coated large nanosheets enter through both CME and phagocytosis. Our findings help reveal the cellular interaction properties of nanosheets and will facilitate biomedical applications of graphene as well as toxicity studies

of these materials. Furthermore, these results provide a much needed understanding of interactions at the interface of two-dimensional nanostructures and biological systems in general.

ASSOCIATED CONTENT

Supporting Information

Additional TEM images, PCGO and GNP-PCGO stability assays, WST-1 cytotoxicity assay, and comparison of uptake quantifications by ICP-MS and flow cytometry. This material is available free of charge via the Internet at <http://pubs.acs.org>.

AUTHOR INFORMATION

Corresponding Author

*Phone: +9014952797. Fax: +9014955715. E-mail: dr.bingyan@gmail.com.

Notes

The authors declare no competing financial interest.

ACKNOWLEDGMENTS

We thank Ms. Lou G. Boykins, Ms. Sharon Frase, and Dr. Yannan Ouyang for technical assistance. We thank Dr. Cherise Guess for the editing service. This work was supported by the National Basic Research Program of China (2010CB933504), National Natural Science Foundation of China (90913006, 21077068, and 21137002), National Cancer Institute (P30CA027165), NIH (CA096832 and CA21765 to MFR), and the American Lebanese Syrian Associated Charities (ALSAC).

REFERENCES

- (1) Geim, A. K.; Novoselov, K. S. *Nat. Mater.* **2007**, *6*, 183–191.
- (2) Feng, L. Z.; Liu, Z. A. *Nanomedicine* **2011**, *6*, 317–324.
- (3) Song, W.; Li, D. W.; Li, Y. T.; Li, Y.; Long, Y. T. *Biosens. Bioelectron.* **2011**, *26*, 3181–3186.
- (4) Sun, X. M.; Liu, Z.; Welscher, K.; Robinson, J. T.; Goodwin, A.; Zaric, S.; Dai, H. J. *Nano Res.* **2008**, *1*, 203–212.
- (5) Zhang, L. M.; Xia, J. G.; Zhao, Q. H.; Liu, L. W.; Zhang, Z. J. *Small* **2010**, *6*, 537–544.
- (6) Yang, K.; Zhang, S. A.; Zhang, G. X.; Sun, X. M.; Lee, S. T.; Liu, Z. A. *Nano Lett.* **2010**, *10*, 3318–3323.
- (7) Zhang, W.; Guo, Z. Y.; Huang, D. Q.; Liu, Z. M.; Guo, X.; Zhong, H. Q. *Biomaterials* **2011**, *32*, 8555–8561.

- (8) Yi, C. Q.; Liu, D. D.; Fong, C. C.; Zhang, J. C.; Yang, M. S. *ACS Nano* **2010**, *4*, 6439–6448.
- (9) Mu, Q. X.; Broughton, D. L.; Yan, B. *Nano Lett.* **2009**, *9*, 4370–4375.
- (10) Mu, Q. X.; Du, G. Q.; Chen, T. S.; Zhang, B.; Yan, B. *ACS Nano* **2009**, *3*, 1139–1144.
- (11) Chithrani, B. D.; Chan, W. C. W. *Nano Lett.* **2007**, *7*, 1542–1550.
- (12) Pantarotto, D.; Singh, R.; McCarthy, D.; Erhardt, M.; Briand, J. P.; Prato, M.; Kostarelos, K.; Bianco, A. *Angew. Chem., Int. Ed.* **2004**, *43*, 5242–5246.
- (13) Zhu, Y. W.; Murali, S.; Cai, W. W.; Li, X. S.; Suk, J. W.; Potts, J. R.; Ruoff, R. S. *Adv. Mater.* **2010**, *22*, 3906–3924.
- (14) Jiang, X. E.; Rucker, C.; Hafner, M.; Brandholt, S.; Dorlich, R. M.; Nienhaus, G. U. *ACS Nano* **2010**, *4*, 6787–6797.
- (15) Liu, C. X.; Yu, W. Y.; Chen, Z. J.; Zhang, J.; Zhang, N. *J. Controlled Release* **2011**, *151*, 162–175.
- (16) Krpetic, Z.; Porta, F.; Caneva, E.; Dal Santo, V.; Scari, G. *Langmuir* **2010**, *26*, 14799–14805.
- (17) Yaron, P. N.; Holt, B. D.; Short, P. A.; Losche, M.; Islam, M. F.; Dahl, K. N. *J. Nanobiotechnol.* **2011**, *9*.
- (18) Kostarelos, K.; Lacerda, L.; Pastorin, G.; Wu, W.; Wieckowski, S.; Luangsivilay, J.; Godefroy, S.; Pantarotto, D.; Briand, J. P.; Muller, S.; Prato, M.; Bianco, A. *Nat. Nanotechnol.* **2007**, *2*, 108–113.
- (19) Shi, X.; von dem Bussche, A.; Hurt, R. H.; Kane, A. B.; Gao, H. *Nat. Nanotechnol.* **2011**, *6*, 714–719.
- (20) Hu, W. B.; Peng, C.; Lv, M.; Li, X. M.; Zhang, Y. J.; Chen, N.; Fan, C. H.; Huang, Q. *ACS Nano* **2011**, *5*, 3693–3700.
- (21) Thorek, D. L. J.; Tsourkas, A. *Biomaterials* **2008**, *29*, 3583–3590.
- (22) Jin, H.; Heller, D. A.; Sharma, R.; Strano, M. S. *ACS Nano* **2009**, *3*, 149–158.
- (23) Oh, W. K.; Kim, S.; Choi, M.; Kim, C.; Jeong, Y. S.; Cho, B. R.; Hahn, J. S.; Jang, J. *ACS Nano* **2010**, *4*, 5301–5313.
- (24) Box, G. E. P.; Cox, D. R. *J. R. Stat. Soc. B Stat. Meth.* **1964**, *26*, 211–252.
- (25) Liu, J. B.; Fu, S. H.; Yuan, B.; Li, Y. L.; Deng, Z. X. *J. Am. Chem. Soc.* **2010**, *132*, 7279–7281.
- (26) Jiao, P. F.; Zhou, H. Y.; Otto, M.; Mu, Q. X.; Li, L. W.; Su, G. X.; Zhang, Y.; Butch, E. R.; Snyder, S. E.; Jiang, G. B.; Yan, B. *J. Am. Chem. Soc.* **2011**, *133*, 13918–13921.
- (27) Zhou, H. Y.; Jiao, P. F.; Yang, L.; Li, X.; Yan, B. *J. Am. Chem. Soc.* **2011**, *133*, 680–682.
- (28) Li, X.; Zhou, H. Y.; Yang, L.; Du, G. Q.; Pai-Panandiker, A. S.; Huang, X. F.; Yan, B. *Biomaterials* **2011**, *32*, 2540–2545.
- (29) Mimura, N.; Asano, A. *Nature* **1976**, *261*, 319–321.
- (30) Charriere, G. M.; Cousin, B.; Arnaud, E.; Saillan-Barreau, C.; Andre, M.; Massoudi, A.; Dani, C.; Penicaud, L.; Casteilla, L. *Exp. Cell Res.* **2006**, *312*, 3205–3214.
- (31) Wang, L. H.; Rothberg, K. G.; Anderson, R. G. W. *J. Cell Biol.* **1993**, *123*, 1107–1117.
- (32) Chang, Y.; Yang, S. T.; Liu, J. H.; Dong, E.; Wang, Y.; Cao, A.; Liu, Y.; Wang, H. *Toxicol. Lett.* **2011**, *200*, 201–210.
- (33) Yang, K.; Wan, J.; Zhang, S.; Tian, B.; Zhang, Y.; Liu, Z. *Biomaterials* **2012**, *33*, 2206–2214.

NOTE ADDED AFTER ASAP PUBLICATION

This paper was published on the Web on March 23, 2012. Additional minor text corrections were added, and the corrected version was reposted on March 27, 2012.